50th AIAA Aerospace Sciences Meeting including the New Horizons Forum and Aerospace Exposition
09 - 12 January 2012, Nashville, Tennessee
AIAA 2012-0354

Experimental Investigation and Numerical Prediction of Thermo-acoustic Instabilities and Associated Liner Vibrations Induced by Combustion Process in Gas Turbines

Artur K. Pozarlik and Jim B. Kok
University of Twente, Laboratory of Thermal Engineering, Enschede,7500AE, The Netherlands

In this paper, lean premixed combustion on natural gas is studied in experimental and numerical way. Experiments are done at the state-of-the-art 500 kW thermal power combustion setup. The test rig resembles combustion chamber of gas turbine and can be pressurised up to 5 bar absolute pressure. The experimental study are applied for validation of numerical computations. For numerical calculations a hybrid approach combining CFD and FEM methods is used. Mutual interaction between acoustic wave propagation inside the combustion chamber and structural vibrations is studied applying acousto-elastic model. During the CFD computations, pressure fluctuations created by the flame in the combustion chamber, are calculated first. The results of the CFD are exported then to the FEM code, where interaction between acoustic waves and wall vibrations is resolved. To reduce the effect of numerical dispersion and dissipation of acoustic waves in the CFD code, only the pressure recorded near the flame region is transferred. To simulate acoustic waves next to the vibrating liner, the investigated model is equipped with acoustic elements designed to recognize a structure on one side and a fluid on the other side of the element. The frequencies at which thermo-acoustic instabilities may appear at given operational conditions are predicted. Furthermore, a modal analysis to mark the hazardous structural, acoustic and coupled modes and eigenfrequencies is performed. Computational results are validated against experimental data. Results are in good agreement.

I. Background

THE main drawback of lean premixed combustion of natural gas in gas turbines is its high sensitivity on thermo-acoustic instabilities. Inside the combustion chamber interaction between four phenomena, namely combustion, acoustics, aerodynamics and vibration of the combustion chamber walls take place. Each flame has intrinsic instabilities which lead to noise generation. Two types of noise generated by flames can be distinguished: the autonomous noise which comes from the instabilities in the turbulent flow field in the flame only and driven noise which is a result of mutual interaction between flame aerodynamics and acoustic waves inside the combustion chamber. The latter is of great importance in design and operation of gas turbine engines as it can lead to heavy thermo-acoustic instabilities and subsequently to damage of the combustion system. The unsteady heat release by the flame is an acoustic source and induces pressure waves in the acoustic resonator. These acoustic waves travel downstream of the chamber and after reflection from the boundaries return to the flame. As a result of the impinging acoustic wave, acoustic velocities are perturbing the burner flows. This way the instabilities within the flame are enhanced and the flame fluctuates even stronger. The unsteady combustion process produces high amplitude acoustic waves which increase vibrations of the liner. This behavior can lead to self-excited oscillations of such high amplitude that fatigue damage of the structural parts is caused.

The relation between a flame and the acoustic field was described first by Lord Rayleigh. He stated that at the moment when heat fluctuations released by the flame are in phase with the pressure fluctuations, i.e. when the phase difference lies between -90^{o} and $+90^{o}$, the thermo-acoustic instabilities are enhanced. On the other hand, the instabilities are damped when heat and pressure oscillations are out of phase[1]. This is known as a Rayleigh's criterion, see *Equation* 1.

It was observed by other authors[2-4] that Rayleigh's criterion is a necessary but not a sufficient condition for the instabilities to occur. Chu[5] introduced changes in the original criterion by taking into account energy losses on the domain boundaries. According to *Equation* 2 the self-exciting instability loop is growing up in

amplitude till the saturation limit when the heat released by the flame and pressure fluctuations are in phase and the energy gain exceeds energy losses on the wall.

$$\int_V \int_0^\tau p'Q'dtdV > 0 \tag{1}$$

$$\frac{(\gamma-1)}{\gamma p_0}\int_V \int_0^\tau p'Q'dtdV > \int_A \int_0^\tau p'\boldsymbol{u}dtdA \tag{2}$$

The origin of combustion instabilities is well known and it is referred to in many publications[6-8]. However, the fundamental mechanisms of the instabilities are difficult to recognize precisely. Oscillations in heat release or pressure fluctuations are produced by countless mechanisms and physical processes which influence each other, thus the exact recognition of the source is in many cases impossible. Fluctuations in equivalence ratio, unsteady strain rate, interactions between flame and vortex or flame-boundaries interaction are a few of them[9]. Also each of the above mentioned processes depends on additional factors. Nozzle geometry, fuel kinetics, heating value, ambient temperature and swirl conditions can cause equivalence ratio fluctuations[7]. These processes generate perturbations in heat release ratio by inducing oscillations in flame position or distortion of the enveloping area of the flame.

Of great importance for the operation of the gas turbine engine is not the noise emitted but its structural integrity. Prediction of the instabilities frequency and conditions at which they will appear are crucial for reliable operation of gas turbine.

II. Combustion Test Rig

The combustion setup under investigation (see Figure ***1***) is intended to be representative for a section of a full scale gas turbine annular combustion chamber. Due to significant geometrical dimensions and high operational costs it is unpractical to build the whole combustion chamber together with its 24 burners. Instead, a slice of the chamber with only one burner and with reduced thermal power is manufactured. In order to obtain similar acoustical and structural eigenfrequencies as during operation on the full scale device, the geometrical dimensions of the investigated setup are matched in scale. The test rig can work with a maximum thermal power equal to 500 kW at 5 bar absolute pressure.

The investigated flame is a natural gas lean premixed preheated flame. Stabilization of the flame is done by inner and outer recirculation regions created by a swirler and sudden expansion of the geometry profile. To decrease the overall temperature of the structural parts exposed to the flame and hot gases, between the liner and pressure vessel a cooling flow is present. Several pressure transducers and thermocouples are located along the setup to monitor temperature and pressure at various locations. Data from the temperature, pressure and flow sensors is collected by LabVIEW[10] and SigLab[11] hardware and software. Further data examination is done with the use of Matlab 7.1 environment[12].

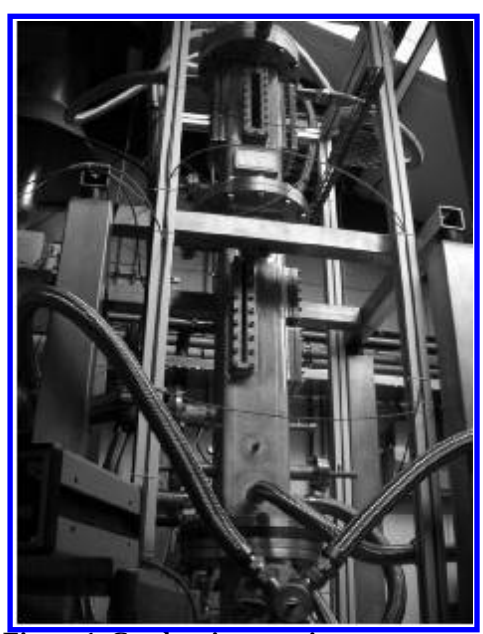

Figure 1. Combustion test rig

The combustion test rig has a modular built. This assures that the individual parts of the setup can be easily disassembled and replaced by new ones, which fit better to the type of research that is conducted at any given time. The main modular parts of the combustion test rig are: the combustion section, structural section and cooling section. Since the configuration of the structural section has a major impact on the liner vibration characteristics, this section is described in details later. First, the other two sections are shortly presented below.

The combustion section is located just behind the burner mouth. In this section combustion process takes place. First the combustible fuel-air mixture is ignited by a spark plug. Then, the flame is self-sustained and stabilized by recirculation regions of hot gas which ignites the fresh mixture. To make observations of the flame the setup is

equipped with a system of windows. The windows are mounted in the liner and pressure vessel. Chemiluminescence and Planer Laser Induced Fluorescence (PLIF) are used to gather information about the flame composition.

The main task of the cooling section is to reduce the temperature of the exhaust gases. In order to do so, the hot flue gases are mixed first with the cool air from the cooling passage and then to decrease their temperature even more, they are sprayed with cold water. Therefore, the gases which leave the setup are cooled down sufficiently to pass the throttle valve and chimney, and finally they can be released to the atmosphere. The second task of the cooling section is to provide a uniform pressure distribution on either sides of the combustion chamber and cooling passage. In account of the small thickness of the liner (1-4mm), the absolute pressure in the combustion chamber must be equal to the pressure inside the cooling passage. Otherwise, high mechanical stresses can occur in the liner walls and finally they might lead to the liner damage. To equalize pressure on both sides of the liner, i.e. in the combustion chamber and cooling passage, the latter is connected with the cooling section by four steel bypass hoses. Since the cooling section is also connected with the combustion chamber, only minor pressure differences between the combustion chamber and cooling passage are possible. Furthermore, at the place where the structural section is connected with the cooling section, a sudden contraction of the combustion chamber exists. This contraction combined with the water spray in the cooling section forced most of the acoustic waves to reflect back inside the combustion chamber and provides at the same time a well-defined acoustic boundary condition for further numerical analysis.

The structural section is the part of the combustion test rig where the vibrations of the liner are measured. To make the liner more sensitive to the pressure changes inside the combustion chamber, part of it has a smaller thickness with comparison to the overall wall thickness. Thus any variations in the pressure pattern inside the combustion test rig are immediately translated to changes in the vibration amplitude and frequency of the flexible section. Furthermore, the flexible section located between much more stiffer and thicker liner parts has well defined structural boundary conditions for the numerical analysis of the structural vibrations.

In order to obtain information about the liner vibrations amplitude and frequency, the flexible section must be able to vibrate freely without any measurement induced damping. Therefore, a non-invasive technique is used for vibration data collection and all thermocouples and pressure transducers are placed at some distance from the flexible section. Since the Laser Doppler Vibrometer is the technique employed for vibration data collection, it is necessary to have access to the vibrating liner via transparent windows. For the liner configuration presented here, the structural modes in the investigated frequency range show mostly the one-dimensional shape. Moreover, the experimental time spent to obtain good two-dimensional data from the square windows is an order of magnitude longer then the time spent for 1D data. Therefore, to reduce recording time, data presented in this paper are for 1D measurements of the liner vibrations through the slit window.

Two liner configurations with different thickness and length of the flexible section are investigated subsequently. The overall size of both is the same, 150/150/1813 mm and 4 mm thickness of the stiff part. The difference lies in the dimensions of the flexible part. In the configuration called Desire, the flexible section thickness is equal to 1.5 mm and has a length of 400 mm, whereas in the Fluistcom configuration, the flexible part has a thickness equal to 1 mm and length equal to 680 mm. The width is always 150 mm. Both names i.e. Desire and Fluistcom come from the names of the European projects during which the liners were manufactured. The Desire liner configuration represents the stiff liner configuration due to smaller and thicker flexible section, while the Fluistcom – the flexible one. The influence of liner configuration on thermo-acoustic instabilities is investigated during the combustion tests at various operating conditions. Both configurations are studied experimentally and numerically under conditions presented in Table 1.

Operating point	Thermal power [kW]	Absolute pressure [bar]	Air factor [-]	Total mass flow rate [g/s]	Preheating temperature [K]
15.7	125	1.5	1.8	75.5	300

Table 1. Operational conditions

III. Numerical Simulations

Acoustic waves resolved using the CFD approach are highly dependent on the time step and grid size resolution. For CFL numbers above unity, acoustic waves which travel through the combustion chamber are partially damped by numerical dissipation and dispersion during the computation process. To avoid restrictions due to the mesh resolution and time step i.e. a fine mesh to simulate the combustion process that would lead to a very small time step in order to resolve the acoustic wave correctly, the acousto-elastic analysis is performed.

In this analysis the combustion process is avoided and instead, pressure fluctuations caused by the oscillating flame are exported to the FEM code where further interaction between vibrating walls and acoustic pressure inside the combustion chamber is investigated. The acousto-elastic interaction is an analysis of the coupling between acoustic waves and elastic structure deformation[13-15]. This analysis is devoted to an investigation of the mutual interaction between moving walls and the acoustic field, which takes place when a thin, light structure is exposed to the acoustic wave. The interaction is most significant when the acoustic fluid is enclosed by the elastic structure. Then acoustic waves induced in the chamber produce an external pressure loads on the wall surface. Changes in the pressure field induce vibrations of the wall. The vibrating structure is another source of acoustic waves and induces pressure fluctuations in the surrounding fluid[16]. As a result of interaction between these waves, the acoustic field inside the cavity can be modified[17].

The acousto-elastic coupling depends on the properties of the medium through which the acoustic wave travels. For air, only compressibility and inertia effects are taken into account. However, in some cases when the acoustic domain is smaller or of the same order as the viscous layer, the viscous effect should be considered. This exception has also application to the thermal boundary layer, which for gases has a similar thickness as the viscosity layer. When both layers are included in the calculations and when the acoustic domain is small, additional energy dissipation is observed by acoustic wave conversion into heat[18,19]. Knowing that the investigated gas is air, and the Reynolds numbers are high, both viscous and thermal boundary layers have minor influence on the acoustic field in the combustion chamber. Thus the viscous and thermal effects are neglected in the computation process presented here.

The acousto-elastic model investigated in this paper considers air at a temperature equal to the temperature of the hot gases inside the combustion chamber. The presence of air trapped by the surrounding structure has its influence. Air introduces additional mass, stiffness and damping, which modifies the performance of a system with vacuum[20].

The acoustic field created by the acoustic source can be divided into two main regions: the near field and the far field acoustics. The near field acoustics is located in the vicinity of the acoustic source and strongly depends on the source properties and distance. The far field zone starts at some distance from the source. Beyond the point of transition between the near field and far field acoustics, the wave distribution is mainly independent on the distance from the source. Several definitions of the transition point between near and far field acoustics exist depending on the relation between dimensions of the source, the wave length, diffraction and the type of the acoustic source[21,22]. The results of the CFD calculation presented in Figure 2 show that in the investigated combustion chamber, at some distance from the monopole source, which is the flame, the pressure fluctuations are one-dimensional. Therefore, it is possible to truncate the acoustic domain and export the mean pressure fluctuations from the CFD calculation to the FEA without contamination of the investigated signal.

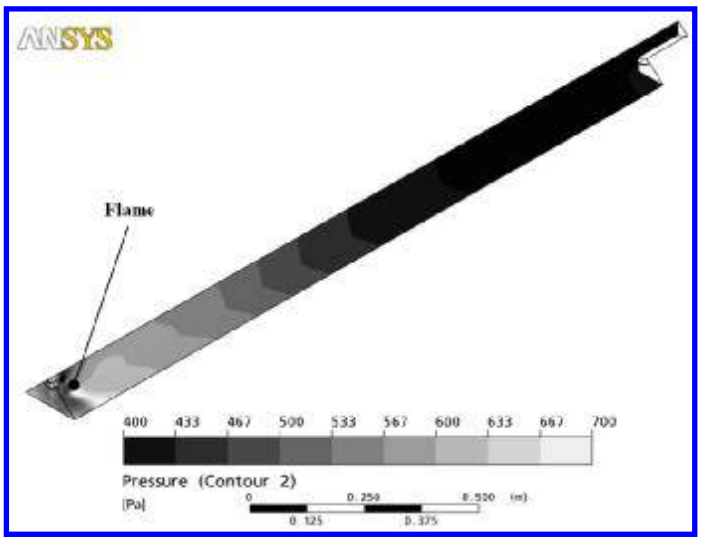

Figure 2. A pattern of typical pressure distribution inside the combustion chamber (from CFD)

Acousto-elastic computations investigated here take also into account the cooling passage. In the cooling passage the flow is not very turbulent and with the absence of a flame, the vibrating walls are the main source of acoustic waves. The experimental and numerical results are also compared there.

For all calculations presented in this paper, the CFD analysis of the combustible flow with time step 1e-4 s is done first in the CFX commercial code. Next, the pressure results from the near flame field are transferred to the FEM code where the wave equation is being solved using acoustic elements designed for this application. This hybrid approach allows combining two separate codes for the investigation. During the acousto-elastic computations, unlike the partitioned fluid-structure analysis, where the exchange of information is performed every time step, the data is transferred after the CFD computations are finished. This procedure reduces the computation time, since the time-consuming data exchange process through the interface connection between the different codes is neglected. Because the truncation is done near the flame front, it is assumed that the transferred acoustic waves are not contaminated by numerical errors and the numerical dissipation and dispersion have minor influence on the acoustic waves. At the location where the truncation is performed, the acoustic waves present already a one-dimensional pattern. Thus, errors introduced during truncation and data transfer between the codes are reduced to a minimum. In the Ansys Multiphysics code, the acoustic waves created by the (flame induced) source in the combustion chamber cavity surrounded by the flexible walls are simulated. The mutual interaction between acoustic waves travelling inside the fluid with vibration of the liner walls is observed. An effect that the modified acoustic waves exert on the flame is not taken into account due to non-availability of combustion and turbulent models in the FEM code. The data exchange process between Ansys CFX and Ansys Multiphysics code is presented schematically in Figure 3**.**

The pressure fluctuations taken from the CFX computation are resolved in the Ansys Multiphysics code using the homogenous wave equation, defined as:

$$\frac{1}{c_0^2}\frac{\partial^2 p'}{\partial t^2} - \frac{\partial^2 p'}{\partial x_i^2} = 0 \qquad (3)$$

Equation 3 is valid for a medium without mean flow and without temperature gradient. Furthermore, viscous effects are neglected and the medium is assumed to be a continuum. Assuming a harmonic wave of shape $p' = p_o e^{i\omega t}$, *Equation* 3 simplifies to the Helmholtz equation defined as:

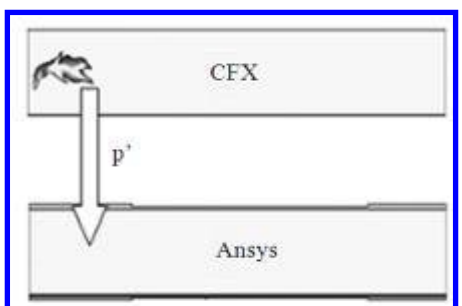

Figure 3. Data transfer from CFD to FEM code

$$k^2 p_0 + \frac{\partial^2 p_0}{\partial x_i^2} = 0 \tag{4}$$

Where: k is a wavenumber, $k = \frac{\omega}{c_0}$

Using the Galerkin procedure for discretization and taking into account dissipation of energy due to damping being present at the fluid boundary *Equation* 5 is obtained.

$$\int_V \delta p' \frac{1}{c^2} \frac{\partial^2 p'}{\partial t^2} dV - \int_V \delta p' \nabla \cdot (\nabla p') dV + \int_S \delta p' \left(\frac{r}{\rho_0 c}\right) \frac{1}{c} \frac{\partial p'}{\partial t} dS = 0 \tag{5}$$

Where: r is the characteristic impedance.

The FEM code employed for the acousto-elastic interaction analysis includes not only acoustic elements for the acoustic pressure waves travelling in the chamber but it is also equipped with solid elements. These elements serve to simulate displacements and stresses inside the walls surrounding the gas cavity[23]. The connection between the fluid and structural domain is modelled using additional elements which recognize the structure on one side and fluid on the other side. The interaction between the fluid and structure at the mesh interface includes the acoustic pressure exerting a force on the structure and the structural motion producing an effective fluid load, according to *Equation* 6 and *Equation* 7.

$$[\boldsymbol{M_S}]\{\ddot{\boldsymbol{U}}\} + [\boldsymbol{C_S}]\{\dot{\boldsymbol{U}}\} + [\boldsymbol{K_S}]\{\boldsymbol{U}\} = \{\boldsymbol{F_S}\} + [\boldsymbol{R}]\{\boldsymbol{P}\} \tag{6}$$

$$[\boldsymbol{M_F}]\{\ddot{\boldsymbol{P}}\} + [\boldsymbol{C_F}]\{\dot{\boldsymbol{P}}\} + [\boldsymbol{K_F}]\{\boldsymbol{P}\} = \{\boldsymbol{F_F}\} - \rho_0 [\boldsymbol{R}]^{\boldsymbol{T}} \{\ddot{\boldsymbol{U}}\} \tag{7}$$

In *Equation* 6 and *Equation* 7, the coupling matrix **R** takes into account the direction of the normal vector defined for each pair of coincident fluid and structural element faces. The positive direction of the normal vector is defined to be outward from the fluid mesh and towards to the structure[23]. $\mathbf{F_S}$ and $\mathbf{F_F}$ are structural and fluid forces, respectively.

Both the structural and fluid load quantities that are produced at the fluid structure interface are functions of unknown nodal degrees of freedom. The governing finite element matrix equations then become:

$$\begin{bmatrix} \boldsymbol{M_S} & \boldsymbol{0} \\ \rho_0 \boldsymbol{R^T} & \boldsymbol{M_F} \end{bmatrix} \begin{bmatrix} \ddot{\boldsymbol{U}} \\ \ddot{\boldsymbol{P}} \end{bmatrix} + \begin{bmatrix} \boldsymbol{C_S} & 0 \\ 0 & \boldsymbol{C_F} \end{bmatrix} \begin{bmatrix} \dot{\boldsymbol{U}} \\ \dot{\boldsymbol{P}} \end{bmatrix} + \begin{bmatrix} \boldsymbol{K_S} & \boldsymbol{-R} \\ 0 & \boldsymbol{K_F} \end{bmatrix} \begin{bmatrix} \boldsymbol{U} \\ \boldsymbol{P} \end{bmatrix} = \begin{bmatrix} \boldsymbol{F_S} \\ \boldsymbol{F_F} \end{bmatrix} \tag{8}$$

As can be seen in the above equation, the nodes on the fluid structure interface are characterized by both the displacement and pressure degrees of freedom.

A. CFD Model

For the reacting flow calculations, the standard CFX single-step model of a reaction is used. The model determines the rate at which a component is consumed or created in a single reaction step during the combustion process. The Eddy Dissipation/Finite Rate Chemistry (ED/FRC) model is applied to calculate reactions occurring in the flame. This model is a combination of the features of two different models, namely the Eddy Dissipation model (ED) and Finite Rate Chemistry (FRC) model. In ED/FRC model, the reaction rate is limited by turbulence quantities or by mixing. Therefore it can be used for calculations in which reaction rates are limited by turbulent mixing in one area of the domain and limited by kinetics somewhere else[24]. Combining the ED and FRC approach allows the ED/FRC model to capture the whole range of Damköhler numbers in the reacting flow. Depending on the local Damköhler number defined as: $Da = \tau_t / \tau_c$, the Eddy Dissipation model (Da>1) or Finite Rate Chemistry model (Da<1) is applied. The effective reaction rate, for the combined model, is computed to be the minimum of the Finite Chemistry Rate and the Eddy Dissipation rate. This procedure is used for each reaction step separately, so while the rate for one step may be limited by the chemical kinetics, some other step might be limited by turbulent mixing at the same time and physical location. The whole range of methane-air flames starting from lean and ending in stoichiometric regime can be calculated with the use of ED/FRC model.

The SAS-SST model as available in the CFX code are used to resolve turbulence. Previous calculations have shown that the SAS-SST model is less dissipative for acoustic energy than the commonly used standard k-ε turbulent model[25,26]. The concept of SAS simulation is based on the introduction of the von Karman length-scale

into the turbulence scale equations. Therefore the SAS-SST models can dynamically change and adjust to resolved structures, which results in behaviour similar to LES calculations in unsteady regions of the flow field[25].

The main target of this work is to describe the mutual interaction between combustion, acoustics and structural vibrations inside the combustion chamber. To investigate simultaneously the interaction between those phenomena, the numerical grid resolution must be dense enough to capture flame features, but on the other hand, because coupling CFD and FEM is a very time-consuming process, the computations cannot take too long. To save computational time and at the same time to increase the number density of elements within the calculated model, the computational domain is reduced to a quarter section of the real combustion chamber, with periodic boundary conditions. A total number of 720 000 unstructured elements is used for the calculations.

The investigated flame is stabilized by two recirculation zones. To capture the flame properties, both recirculation regions should be predicted accurately. Therefore most of the elements used for the numerical model are placed in the flame and recirculation region zones. Behind this region the mesh has a lower density. The near-wall region is created with the use of prism elements to avoid generating highly distorted tetrahedral elements at the face. The velocity and turbulence profiles at the inlet of the combustion chamber are taken from steady-state calculations of the geometry including the pressure decouplers and plenum area. For the transient combustion calculations, forced oscillations are investigated. The fuel to air equivalence ratio is oscillating with frequency of 300 Hz and amplitude equal to 8.5% of the mean. On the wall, where structural vibrations are investigated, a heat transfer coefficient is imposed. Other walls have adiabatic no-slip boundary conditions. The influence of the pressure fluctuations in the cooling passage are neglected. The combustion process is investigated at the exact same operating conditions as during the experimental tests. Computational domain and temperature profile are presented in Figure 4.

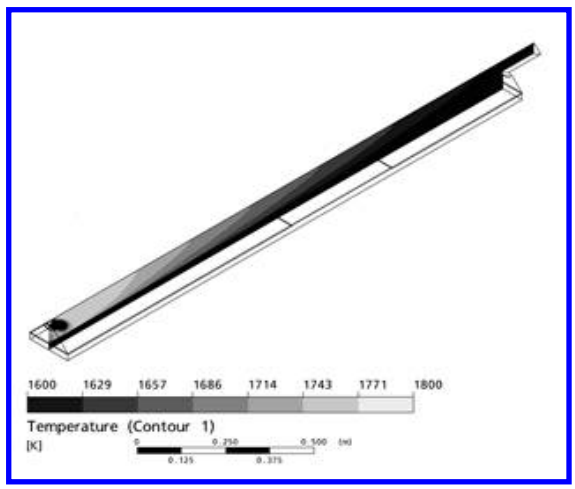

Figure 4. CFD computational domain and temperature profile

B. Acousto-elastic model

The spatially averaged pressure fluctuations in the CFX calculations are taken from the near flame region and implemented to the acousto-elastic model as boundary conditions. The combustion chamber geometry is simplified to a rectangular shape without the burner and exhaust pipe. A boundary absorption coefficient $\beta = \frac{r}{\rho_0 c}$ is calculated based on changes in the cross-section area and imposed as the outlet boundary conditions. At the inlet, an acoustically hard wall is imposed. Three different types of elements are used. For the structural modelling, SHELL63 elements with the element real constant equal to the thickness of the individual liner sections are employed. The SHELL63 elements are based on the Kirchhoff-Love theory[27]. The transverse shear stresses are not taken into account. Due to the small ratio between the thickness of the liner wall and other wall dimensions (always below 0.1) and due to a bending stress which changes linearly with the body thickness, the Kirchhoff-Love theory is valid for the liner configuration presented here. The air cavities of the combustion chamber and cooling passage are represented by the FLUID30 acoustic elements. Two types of FLUID30 elements are used. The major part of the acoustic domain is modelled with regular FLUID30 acoustic elements. One layer of the FLUID30 elements, with ability to recognize structure on one side and fluid on the other, is placed next to the wall. The governing acoustic equation is discretized taking into account the coupling between acoustic pressure and structural motion at the interface, see *Equation* 8. Moreover, for the case with cooling passage geometry, in order to prevent direct connection of the pressure nodes from the combustion chamber with nodes from the cooling passage at the structure interface, the model of the liner is divided into two equal parts. These parts are connected together by stiff degrees of freedom and they have exactly the same properties as the original model. Therefore, any change in one of the structural sections forces the same behaviour in the other section. This configuration assures correct transfer of loads between the acoustic fluid and structural elements. The cross-section of the numerical model with pointed different types of elements and connections is presented in Figure 5.

The model includes all four liner walls. The walls are clamped on both ends. Material properties of the stainless steel are adequate to wall temperature of 760°C. The temperature field inside the combustion chamber is equal to the average temperature calculated during the CFD analysis. The speed of sound inside the combustion chamber and in cooling passage is taken at the average temperature field, observed during previous research. Physical damping is not included into the computation model. However, the liner vibrations can be affected by air resistance inside the combustion chamber. The effect of added stiffness and mass are taken into account. In case of the model with the cooling passage, additional damping can be provided by the cooling flow. A longitudinal cross-section of the numerical model geometry (without cooling passage) together with the boundary conditions is presented in Figure 6. Two different liner configurations are investigated: the Fluistcom configuration with thin and long flexible part and the Desire configuration with a stiff flexible part.

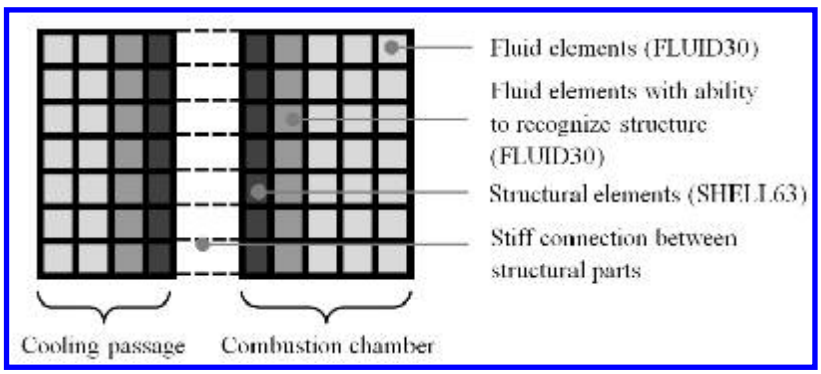

Figure 5. Transverse cross-section of the acousto-elastic model

C. Modal Analysis

To determine the vibration characteristics of the combustion chamber walls and the influence of the hot gases trapped inside, a modal analysis is performed. The eigenfrequencies and shapes of the structural, acoustics and coupled modes are compared to each other and a relation between them is observed.

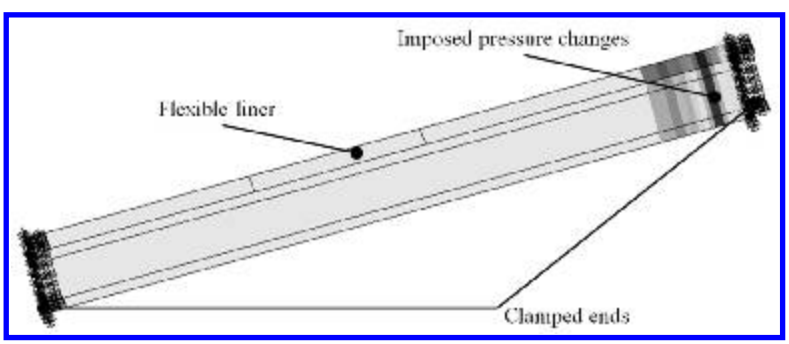

Figure 6. Numerical acousto-elastic model with boundary conditions (for better visibility the cooling passage is not included)

The same numerical model as for the acousto-elastic analysis is employed to investigate the coupled modes. The difference lies only in the boundary conditions used for the model. For the modes investigation there is no need to transfer pressure fluctuations from the CFX code, therefore this data is not included in the modal analysis. Also the impedance at the outlet from the combustion chamber is not taken into account. Computations of the coupled modes include structural and fluid domains together. The structural domain has clamped conditions on the top and bottom edges. For the acoustic modes investigation, the numerical domain is reduced to a fluid part only surrounded by acoustically hard walls. This configuration assures full reflection of acoustic waves without possibility of the liner walls to vibrate.

In the coupled modes analysis, the points where the structural and acoustic eigenfrequencies intersect are called isochronism points. The isochronism points are hazardous for combustion systems because the acoustic and structural eigenfrequencies can be fed simultaneously and they can finally lead to unstable combustion and to liner failure.

For both geometries, i.e. Desire and Fluistcom, the total length of the liner and its cross section area are kept unchanged. Due to the assumption of acoustically hard walls, the acoustic mode shape and natural frequencies stay the same for both models. In case of coupled modal analysis, the influence of the flexible section located between the stiff liner parts is observed. This section is different with respect to the length and thickness for both models. The frequencies of the isochronism points are similar for both geometries, however, different structural modes are observed in the vicinity of the isochronism point. Thus the effect of the coupled modes on the system behavior can be different.

IV. Numerical results

The results of the acousto-elastic and modal analysis are presented here in two sections, one for the Desire combustion chamber configuration and a second for the Fluistcom geometry. Furthermore, these results are divided into acousto-elastic results and modal analysis. In both cases the geometries with combustion chamber only and with combustion chamber and cooling passage are discussed. All numerical data is compared with experimental results.

A. DESIRE – Acousto-elastic analysis

Two different geometries i.e. with and without cooling passage are investigated during the acousto-elastic analysis of the Desire configuration. As can be seen in Figure 7, the amplitude of pressure changes during both acousto-elastic computations agrees well with the experimental results.

Also the frequency of main instabilities is predicted correctly. The experimental peaks predicted at 300 Hz, 439 Hz and 640 Hz are visible in the spectrum. The forcing frequency of 300 Hz is the dominant peak. Primary instabilities are predicted by the model at 450 Hz and a secondary at 625 Hz, which gives in both investigated cases a percentage error below 3%. The instabilities predicted by the numerical scheme at 250 Hz are not visible in the experimental spectrum due to feedback from the acoustic field to the flame. Since the acousto-elastic analysis the flame is not modeled this feedback is not included as well. However, the thermo-acoustic instabilities under some circumstances can occur during experiment at two possible frequencies, 441 Hz and 239 Hz[28]. The latter frequency is pointed by the acousto-elastic model at 250 Hz. In the acousto-elastic analysis the forcing peak dominates the thermo-acoustic instabilities, which is not the case for experiment. Improvement of the pressure signal resolved by the CFD code, as well as introduction of the pressure source which depends on the incoming wave should improve obtained results.

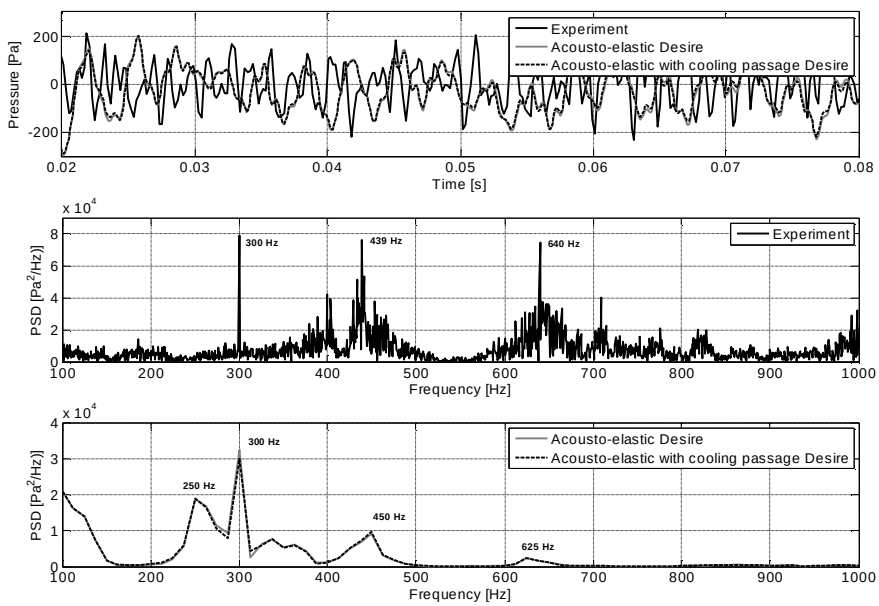

Figure 7. Comparison of the numerical pressure data with experimental results for the acousto-elastic analysis

In the velocity field, both the experimental and numerical data show similar fluctuation amplitudes, see Figure 8.

The forcing frequency at 300 Hz and instability frequency at 439 Hz are present in the numerical spectrum. The forcing frequency predicted by the hybrid approach is exactly at 300 Hz and the vibrations coming from the thermo-acoustic instabilities are placed at 425 Hz. This gives an error less than 3% in case of the prediction of instabilities Similar to the pressure results, also here the dominant peak comes mainly from the forcing frequency. The instability presented in the numerical pressure spectrum at 250 Hz is hardly visible in the velocity spectrum. However, at this frequency there is no coupling between acoustic mode and structural mode, see Table 3 and discussion about modes, thus the effect of pressure changes on the vibration pattern is insignificant.

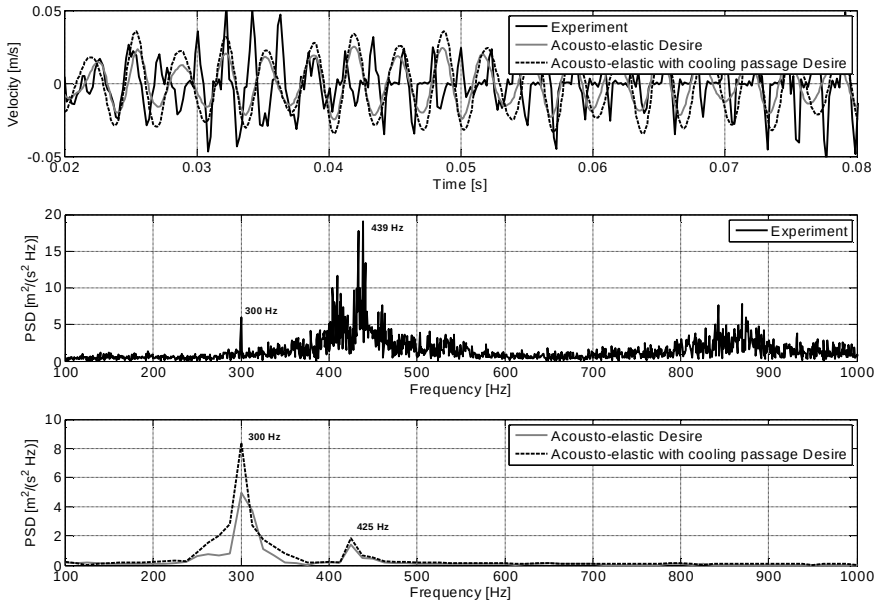

Figure 8. Comparison of the numerical velocity with the velocity obtained during the experiment

Only minor differences between results for model with and without cooling passage are observed, see Figure 7 and Figure 8. Both models predicted the same amplitude of pressure fluctuations and frequency of the instabilities (it is difficult to distinguish the numerical profiles since they are on top of each other). More differences are visible in case of the velocity results, where the additional mass of air induces more significant vibrations of the liner. However, these changes are not translated to a frequency shift. Also they do not induce additional pressure changes in the acoustic and velocity fields. Thus both models predicted the same instability frequency at 425 Hz.

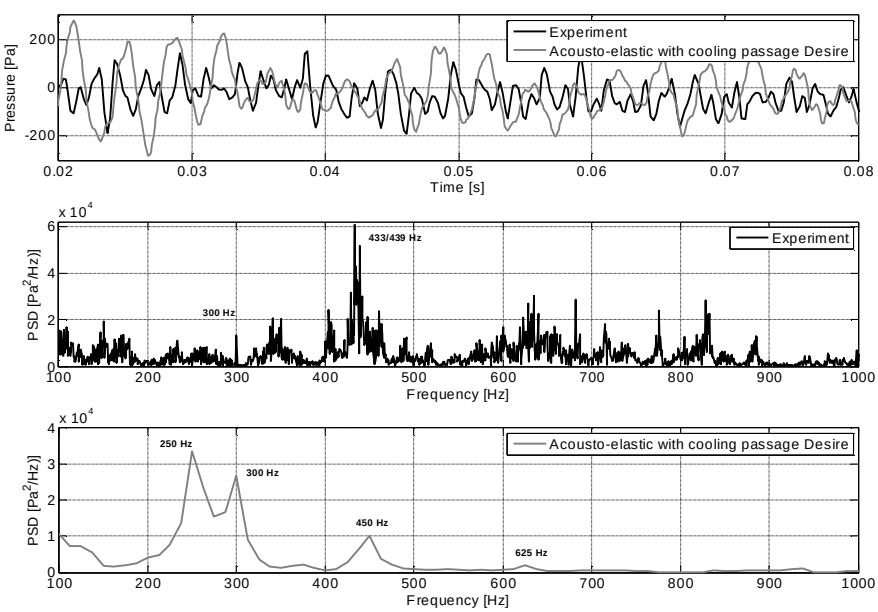

Figure 9. Experimental and numerical pressure inside the cooling passage

Since the flame is not present in the cooling channel and the flow of the coolant is not very turbulent, the acoustic waves present in the cooling channel are created mainly by the vibrating walls and sound transmission by connected channels. In Figure 9, experimental and numerical data of pressure oscillations is presented. The amplitude of the pressure fluctuations predicted by the numerical code is slightly higher than the experimental.

It suggest that in the experimental setup the acoustic wave is damped more than in the numerical model. Here pre-stress and additional stiffness from the welded metal parts test rig have influence. However, as mentioned earlier, a damping coefficient is not included in the material properties of the liner walls, and therefore the abovementioned effect is not taken into account. The main frequencies observed during experiment and computations in the cooling passage cavity are related more to the pressure changes inside the combustion chamber than to the frequencies of the vibrating flexible walls. This behaviour indicates that a significant part of the acoustic waves can travel to the cooling passage by the bypass connection between cooling passage and cooling chamber. Examination of the vibration of the stiff liner part at the location where pressure transducer is located shows that the vibration pattern here is different from the flexible section, see Figure 10.

Moreover, this vibration pattern resembles more the acoustic wave recorded in the cooling passage. Most likely, the acoustic waves created inside the cooling passage are a product of the entire structure which vibrates, and not only of the flexible part. Additionally, connections of pressure transducers, thermocouples and the construction of the bypass between cooling passage and cooling chamber induce additional acoustic effect.

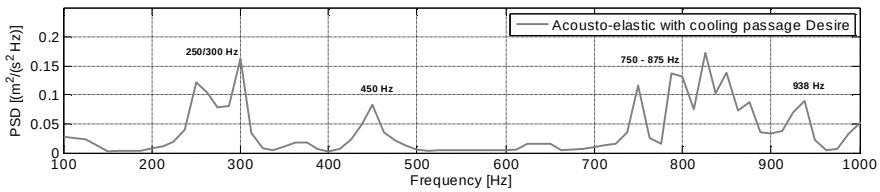

Figure 10. Velocity spectrum at position of pressure transducer

B. FLUISTCOM – Acousto-elastic analysis

In this section the Fluistcom liner configuration is investigated. The more flexible liner section should be able to change the pressure distribution over the liner. As it is shown in Figure 7 and Figure 11 only minor pressure differences, between the Desire and Fluistcom configuration, due to the vibrating liner, are observed in the combustion chamber during numerical computations.

This behaviour suggests that vibrating walls have only a local effect on the pressure field and this effect is not translated to the pressure changes in the upstream part of the combustion chamber. Thus, interaction between the acoustic wave induced by the flame and the one coming from the vibrating walls resembles an evanescent wave. Also experimental results of both liner configurations are very similar. Therefore, the acousto-elastic analysis of the Fluistcom configuration presents similar errors as the acousto-elastic analysis of the Desire liner geometry presented in the previous section. This means that the forcing peak is exactly at the position of the experimental one, and the primary and secondary instabilities are predicted with small error, with respect to the experimental results.

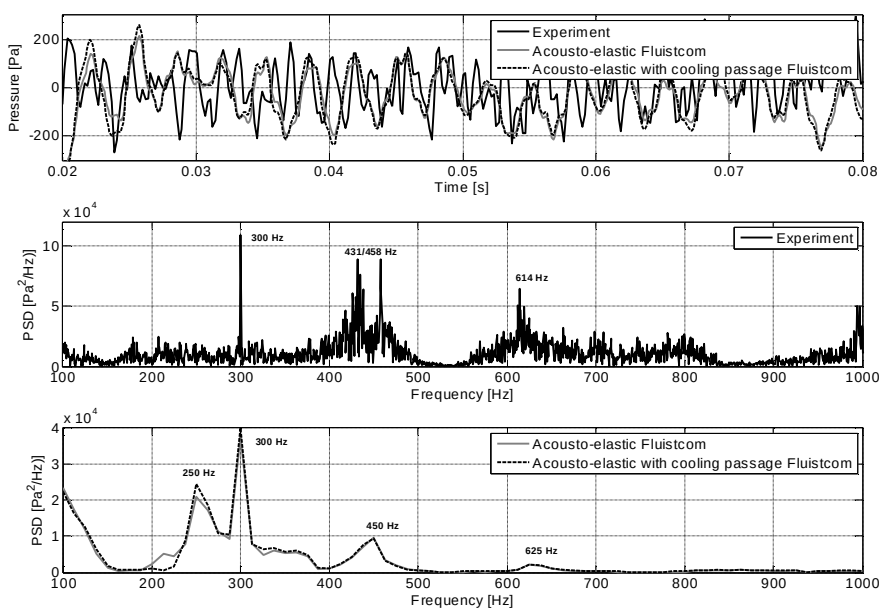

Figure 11. Comparison of the numerical pressure data with experimental results for Fluistcom liner configuration

The wall velocity amplitude predicted by the acousto-elastic models with and without cooling passage is under-predicted with respect to the experimental results (based on RMS values), see Figure 12. Nevertheless, the acousto-elastic model including the cooling passage places the main vibration frequency at 438 Hz. This is in the vicinity of the major experimental velocity peak located at 417 Hz. The acousto-elastic model without cooling passage missed this frequency of vibrations entirely. Thus, the vibrations at 438 Hz are induced by local pressure changes inside the combustion chamber in the neighbourhood of the vibrating wall.

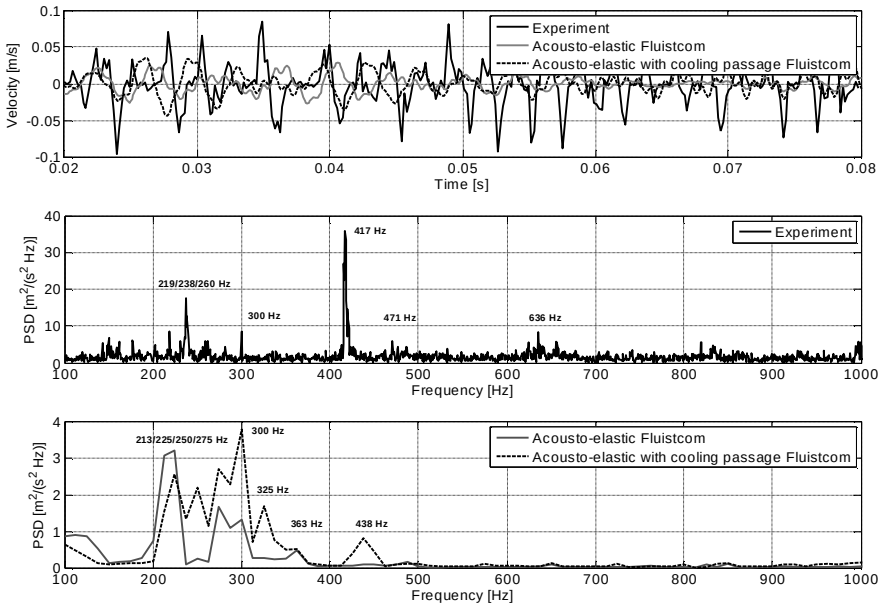

Figure 12. Comparison of the numerical velocity data with experimental results for Fluistcom liner configuration

The remaining frequencies of vibrations in both models are predicted similarly. The forcing frequency is located at 300 Hz which is also exactly the case of the experimental setup. Furthermore, in the range 200 Hz – 300 Hz, several velocity peaks are predicted at frequencies 213 Hz, 225 Hz, 250 Hz and 275 Hz. During the experiment the observed vibrations in this frequency range are pointed at 219 Hz, 238 Hz and 260 Hz, which is in good agreement with the numerical data.

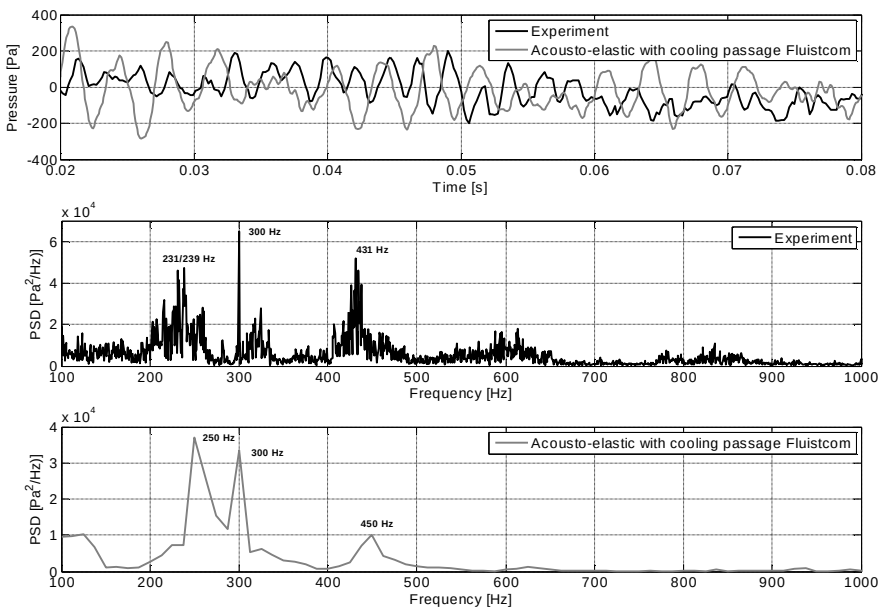

Figure 13. Pressure comparison in the cooling passage

In the cooling passage the main pressure oscillations are predicted well by the acousto-elastic model, see **Error! Reference source not found.**. The instabilities at 239 Hz and 431 Hz are predicted by the model at 250 Hz and 450 Hz, respectively. Similar to the Desire configuration, also here the acoustic waves in the cooling passage are induced by entire wall vibration, see Figure 14. However, the participation of the flexible part in this process is more significant.

C. Modal Analysis of DESIRE

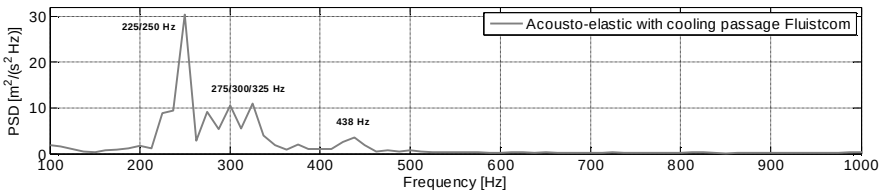

Figure 14: Liner velocity spectrum at location of pressure transducer

Next to the acousto-elastic analysis, the computation of acoustic and coupled modes is performed. Due to the assumption that the wall thickness has no influence on the pressure field inside the combustion chamber, the acoustic modes are the same for the Desire and Fluistcom liner configuration. Furthermore, since the combustion chamber geometry is characterized by high a ratio between length and width/depth of the walls, acoustic modes in the investigated frequency range (up to 1000 Hz) present only longitudinal shape.

Four acoustic modes are distinguished in the investigated frequency range. They are presented in Table 2 and Figure 15. The modes show a different pressure pattern over the combustion chamber. The first acoustic mode at 222 Hz has a uniform pressure distribution over the length. This mode represents a half of the acoustic wave in longitudinal direction. The other acoustic modes show a pattern of one acoustic wave, one and a half acoustic wave and two acoustic waves, respectively, see Figure 15. Depending on the number of half waves in the longitudinal direction, the acoustic modes are numbered as 1a, 2a etc., and structural modes as 1s, 2s etc. The acoustic modes presenting local air compression or rarefaction (modes 2a, 3a etc.) are hazardous. These modes are particularly dangerous, because local significant pressure changes are able to induce strong liner vibrations.

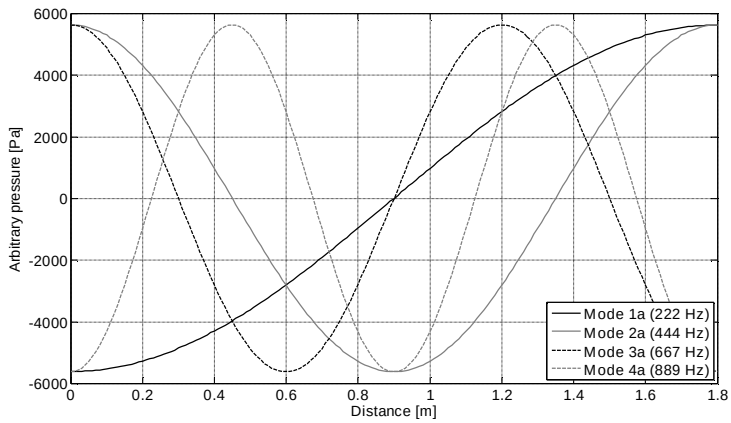

Figure 15. Acoustic modes (pressure distribution along centreline)

Mode number	1	2	3	4
Eigenfrequency [Hz]	222	444	667	889

Table 2. Acoustic eigenfrequencies of the combustion chamber

The influence of the acoustic modes on the liner structure and vice versa is taken into consideration in the coupled modes analysis. During the coupled modes computations the structural domain is coupled with the fluid cavities according to the scheme explained in the earlier part of this paper. Since the number of modes in the frequency range up to 1000 Hz can be significant, the analysis is restricted to the first fifty coupled modes. During the coupling modal analysis of the Desire model, due to the possible interaction between acoustic and structural modes, mainly the modes in the vicinity of the isochronism frequencies are examined. Furthermore, modes which present global longitudinal pressure changes are taken into consideration. The pressure distribution inside the combustion chamber and the liner displacement pattern of the chosen modes are presented in Figure 16 and Figure 17, respectively. Furthermore, in Table 3 the natural frequencies of the modes are listed.

The most energetic modes giving the strongest feedback to the system are the coupled modes, which present significant air compression or rarefaction in the vicinity of the flexible section. These volumetric or synchronized modes are characterized by major volume changes. In the investigated combustion chamber configuration the synchronized modes appear at frequencies of 429 Hz, 446 Hz, 657 Hz and 670 Hz. Two first modes located at 429 Hz and 446 Hz present a symmetrical pressure distribution with one local air rarefaction or compression (thus pattern of 2a symmetrical mode). Two other located at 657 Hz and 670 Hz are unsymmetrical 3a modes, see Figure 16 and Table 3. The four modes are coupled only with symmetrical structural modes (3s and 5s), as presented in Figure 17. It is expected that abovementioned modes can lead to high amplitude oscillation when they are excited.

Mode number	1	2	3	4	5	6	7	8
Eigenfrequency [Hz]	219	312	354	**429**	**446**	542	**657**	**670**

Table 3. Eigenfrequencies of selected coupled modes

At a frequency equal to 219 Hz another isochronism point exists. The structural mode at that frequency is coupled with an acoustic mode. As it was explained above, this acoustic mode due to the uniform pressure distribution gives only minor feedback to the system.

The other modes at 312 Hz, 354 Hz and 542 Hz are modes dominated by the structure but they present a similar pressure distribution as the acoustic modes. However, because there is no acoustic mode in the vicinity, these modes present only a weak coupling between structural and fluid domain. As a consequence, they do not have a significant influence on the thermo-acoustic instabilities.

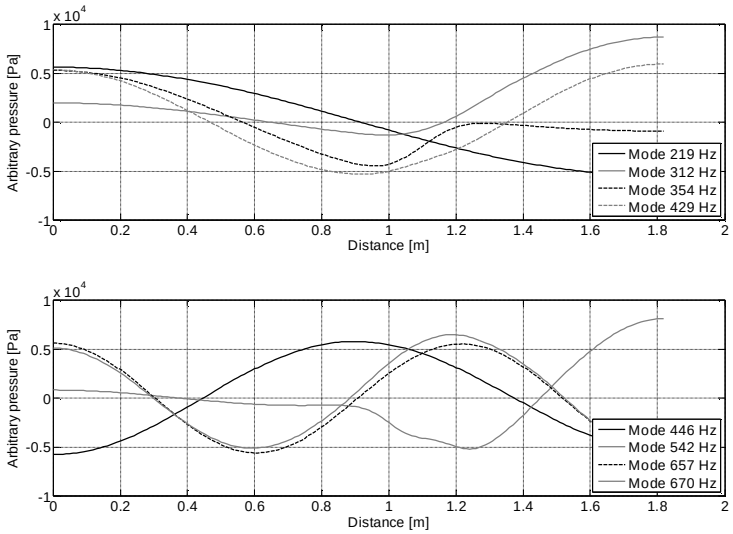

Figure 16. Selected coupled modes (pressure distribution pattern along centreline)

Mapping the modal results onto the experimental pressure spectrum it is found that synchronized modes cover the regions where instabilities occur, see Figure 18. The main instability peak is located directly between two synchronized modes at 439 Hz. The secondary instability is located around 660 Hz. The predicted instability is shifted more towards the high frequency range than the one obtained during the experiment (at 640 Hz). The error can be caused by the assumption of uniform speed of sound within the combustion chamber which is not the case during the experiment. Thermal stresses and pre-stress in the liner are not taken into account, but they may change the mode spectrum as well. The influence of the welds made during the liner manufacturing can have a direct impact on the structural modes, thus also affect the coupled modes.

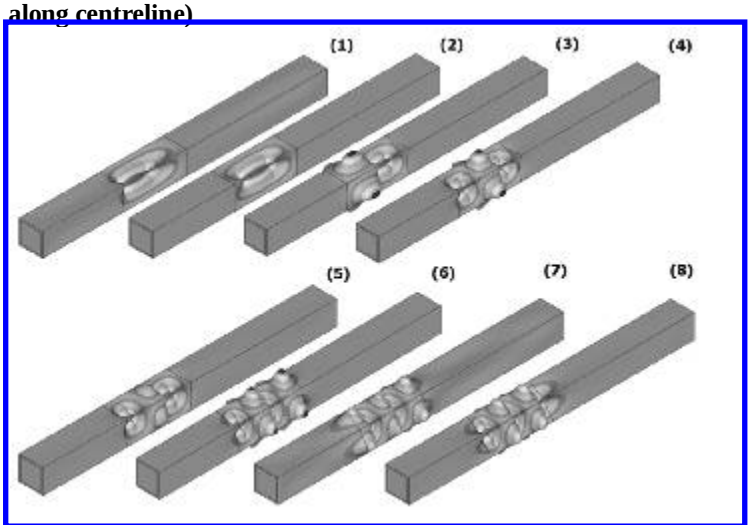

Figure 17. Selected coupled modes (structural pattern)

D. Modal Analysis of FLUISTCOM

Since the acoustic modes are exactly the same for both: Fluistcom and Desire liner configuration, in this section only the coupled modes of the Fluistcom geometry are

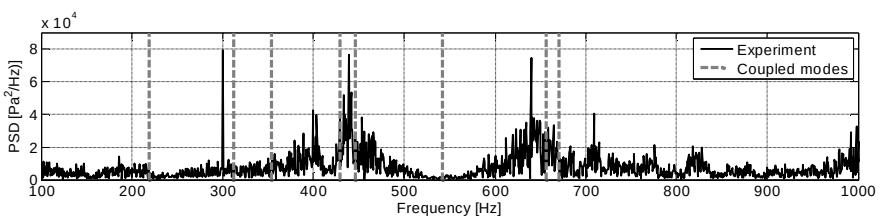

Figure 18. Comparison of the experimental results of pressure with data from modal analysis

considered.

In the investigated frequency range, ten coupled modes which present a potentially hazardous pressure pattern are found. In comparison to the Desire configuration, due to lower liner stiffness, the number of possible hazardous frequencies increased about a factor of two. These coupled modes are listed in Table 4 and presented in Figure 19.

Number	1	2	3	4	5	6	7	8	9	10
Eigenfrequency [Hz]	194	207	223	236	249	280	320	370	**428**	**445**

Table 4. Eigenfrequencies of the Fluistcom coupled modes

The most energetic modes found during the modal analysis are the synchronized ones at frequencies of 428 Hz and 445 Hz. These two modes are located in the vicinity of main acoustic instabilities, see Figure 21. In contrast to the stiff liner configuration, both are coupled here with unsymmetrical structural modes (8s), see Figure 20. However, the shape change of the structural modes does not influence the thermo-acoustic instabilities. This behaviour shows that the instabilities are closely related to the location and shape of the acoustic modes and the influence of the structural modes in the investigated case is minor.

The rest of the possibly hazardous coupled modes have source in the structural vibrations. Therefore their effect on the thermo-acoustic instabilities is not significant. Only the mode with eigenfrequency of 223 Hz is created as a result of coupling of the structural mode with the first acoustic mode. Similar to the Desire configuration, the contribution of this mode to pressure instabilities is weak. Nevertheless, due to the very flexible liner configuration, the influence of the first acoustic mode combined with the structural modes (1s-4s), it is visible on the experimental spectrum of the velocity signal, see Figure 21 *(bottom).*

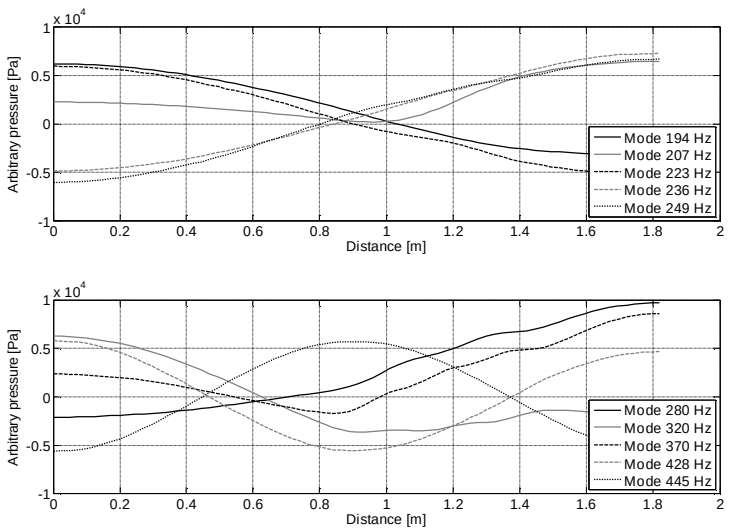

Figure 19. Coupled modes (pressure pattern)

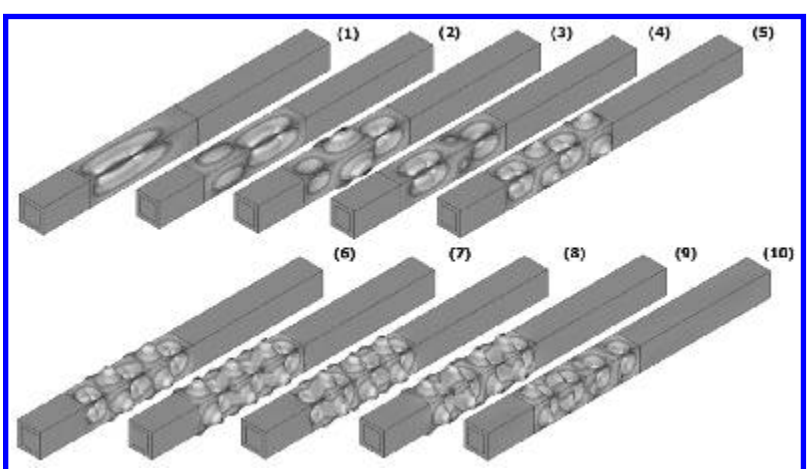

Figure 20. Coupled modes (displacement pattern)

V. Conclusion

The acousto-elastic and modal analysis are presented in this paper for two different configurations of the combustion system. For the acousto-elastic calculation a hybrid approach was used. In this approach the pressure field is calculated first in the CFD code. Then the recorded signal is transferred to the FEM code for further analysis. During the FEM interaction between acoustic waves and vibrating walls is observed. In the modal analysis the influence of the coupled structural and acoustic field on the eigenmodes and eigenfrequencies is investigated.

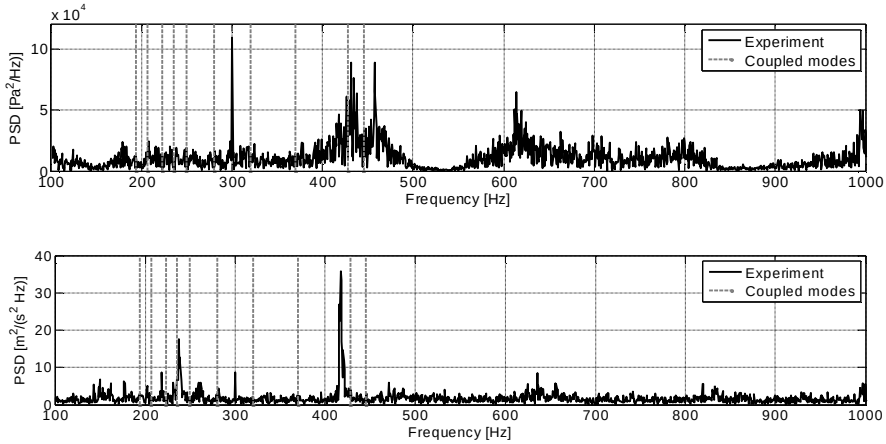

Figure 21. Acoustic and coupled modes mapped on pressure (top) and velocity (bottom) spectrum

The acousto-elastic analysis shows good agreement of the numerical and experimental results. The amplitude of pressure changes is predicted almost exactly by the numerical scheme, whereas the velocity amplitude shows a minor under-prediction of the experimental results.

The main frequency of pressure and velocity oscillations is marked by the acousto-elastic model correctly. Next to the forcing frequency visible at all spectra at 300 Hz, the main instabilities are predicted with an error below 3% for the pressure spectrum and 5% for the velocity spectrum. Also the secondary instabilities, when they appear, are characterized by a similar error. An exception is the acousto-elastic analysis of the Fluistcom liner configuration without cooling passage, which did not show the main velocity peak in the vicinity of 417 Hz. Therefore, for the simulations with the use of very flexible walls it is preferred to use the model with the cooling passage included. This model gives additional mass, stiffness and damping into the system which have influence on the system performance.

Due to the implementation of the cooling channel domain into the computation process it was possible to compare pressure signals inside the cooling channel obtained during the numerical and experimental investigation. Also in this case the numerical results predicted the experimental behavior well.

The difference in the pressure signal between all four acousto-elastic models i.e. Desire and Fluistcom, with and without cooling passage is minor. Increasing the liner flexibility and introducing the cooling passage have impact only on the liner vibration amplitude and frequency.

In case of modal analysis, the most energetic modes which give significant feedback to the system are the synchronized modes. For the combustion chamber configurations investigated in this paper the synchronized modes are located in the vicinity of the second acoustic mode.

Acknowledgment

The authors acknowledge the use of ANSYS and the support by dr. Phil Stopford.

References

Periodicals

[1]Rayleigh, J. (1878). The Explanation of Certain Acoustic Phenomena. *Nature, 18*, 319-321.

[2]Polifke, W., Poncet, A., Paschereit, C., & Doebbeling, K. (2001). Reconstruction of acoustic transfer matrices by instationary computational fluid dynamics. *Journal of Sound and Vibration, 245(3)*, 483-510.

[3]Nicoud, F., & Poinsot, T. (2005). Thermoacoustic instabilities: Should the Rayleigh criterion be extended to include entropy changes. *Combustion and Flame, 142(1)*, 153-159.

[5]Chu, B. (1964). On the energy transfer to small disturbances in fluid flow (Part 1). *Acta Mechanica, 1*(3), 215-234.

[6]Lieuwen, T. (2003). Combustion Driven Oscillations in Gas Turbines. *Turbomachinery International, 44*, 16-18.

[7]Cho, J., & Lieuwen, T. (2005). Laminar premixed flame response to equivalence ratio oscillations. *Combustion and Flame, 140*, 116-129.
[8]Hubbard, S., & Dowling, A. (2001). Acoustic Resonances of an Industrial Gas Turbine Combustion System. *Journal of Engineering for Gas Turbines and Power, 123*, 766-773.
[9]Ducruix, S., Schuller, T., Durox, D., & Candel, S. (2003). Combustion Dynamics and Instabilities: Elementary Coupling and Driving Mechanisms. *Journal of Propulsion and Power, 19*, 722-734.
[14]Breard, C., Sayma, A., Vahdati, M., & Imregun, M. (2002). Aeroelasticity analysis of an industrial gas turbine combustor using a simplified combustion model. *Journal of Fluids and Structures, 16(8)*, 1111-1126.
[19]Fox, M. J., & Whitton, P. N. (1980). The damping of structural vibration by thin gas films. *Journall of sound and vibration, 73*(2), 279-295.
[27]Belov, A. V., Kaplunov, J. D., & Nolde, E. V. (1999). A Refined Asymptotic Model of Fluid-Structure Interaction in Scattering by Elastic Shells. *Flow, Turbulence and Combustion, 61*, 255-267.

Books
[4]Poinsot, T., & Veynante, D. (2005). *Theoretical and Numerical Combustion* . R.T. Edwards, Inc.
[21]Dowling, A. P., & Ffowcs Williams, J. E. (1983). *Sound and sources of sound*. Chichester: Ellis Horwood Publishers.
[22]Crighton, D. G., Dowling, A. P., Ffowcs Williams, J. E., Heckl, M., & Leppington, F. G. (1996). *Modern Methods in Analytical Acoustics*. London: Springer-Verlag.

Proceedings
[16]Kaczor, A., & Sygulski, R. (2005). Free vibration analysis of floating plates. *6th International Conference 'ENVIRONMENTAL ENGINEERING'*, (pp. 774-777). Vilnius.
[25]Menter, F., & Egorov, Y. (2007). Turbulence Modeling of Aerodynamic Flows. Paris: International Aerospace CFD conference.
[26]Pozarlik, A. K., & Kok, J. B. (2008). Numerical prediction of interaction between combustion, acoustics and vibration in gas turbines. *Acousitcs 08* (pp. 2749-2754). Paris: Acoustics 08.

Reports, Theses, and Individual Papers
[13]Huls, R. (2006). *Acousto-Elastic Interaction in Combustion Chambers*. Enschede: PhD thesis.
[15]Hannink, M. (2007). *Acoustic resonators for the reduction of sound radiation and transmission*. Enschede: PhD thesis, University of Twente.
[17]Davis, R. (2008). *Techniques to assess acoustic-structure interaction in liquid rocket engines*. Durham: PhD thesis, Duke University.
[18]Beltman, W. M. (1998). *Viscothermal Wave Propagation Including Acousto-Elastic Interaction*. Enschede: PhD thesis, University of Twente.
[20]Basten, T. G. (2001). *Noise reduction by viscothermal acousto-elastic interaction in double wall panels*. Enschede: PhD thesis, University of Twente.
[28]Van Kampen, J. (2006). *Acoustic pressure oscillations induced by confined turbulent premixed natural gas flames*. Enschede: PhD thesis, University of Twente.

Electronic Publications
[11]DSP-SigLab. (2001). *User Guide*. Spectral Dynamic Inc.

Computer Software
[10]National Instrument, C. (2003). *LabVIEW User Manual*. Austin: National Instrument Corporate.
[12]The MathWorks, I. (2005). *Matlab 7 User Guide*. The MathWorks, Inc.
[23]Ansys. (2007). *HTML Online Documentation*. Ansys Inc.: Ansys 11.
[24]CFX Ansys 11. (2007). *HTML Online Documentation*.